Modelling and Optimization of a Magnetic Spring Based Electromagnetic Vibration Energy Harvester

Liao, H., Ye, T., Pang, Y., Feeney, C., Liu, L., Zhang, Z., Saha, C. & Wang, N.

DOI 10.1007/s42835-021-00904-4
ISSN 1975-0102
ESSN 2093-7423

Publisher: Springer

The final publication is available at Springer via http://dx.doi.org/10.1007/s42835-021-00904-4

Modelling and Optimization of a Magnetic Spring Based Electromagnetic Vibration Energy Harvester

Haojun Liao[1], Tingcong Ye[2*], Yu Pang[1], Ciaran Feeney[1], Lei Liu[1], Zhengmin Zhang[1], Chitta Saha[3], Ningning Wang[1*]

1. College of Electronics and Information Engineering, Hangzhou Dianzi University, Hangzhou, China
2. School of cyberspace, Hangzhou Dianzi University, Hangzhou, China
3. Department of Computing, Electronics and Mathematics， Coventry University, Coventry, UK

Corresponding author: Ningning Wang, ning.wang@hdu.edu.cn; Tingcong Ye, tingcong.ye@hdu.edu.cn

Abstract

This paper presents the development of an AA battery size electromagnetic vibration energy harvester with an aim to maximize the output power density. A tube shape and stacked opposing permanent magnets with magnetic spring were used to suit the shape constraint as well as to achieve high flux linkages. An initial prototype of electromagnetic vibration harvester with AA battery size was built and tested on a controllable shaker to obtain its output voltage and power level at different frequencies for fixed accelerations. A single magnet was fixed at the bottom of the harvester to provide levitation force in this development in order to lower the resonant frequency. A special time-domain based analytical model was also developed using both Finite Element Analysis (FEA) and Simulink simulation. The time-domain analytical model is easier to implement than other frequency domain based analytical models which generally applied in literatures for modelling of the electromagnetic vibration energy harvesters. The analytical model was verified by the measured results obtained from the initial prototype. The validated analytical model was successfully applied to optimize the harvester. Two more generator prototypes were further built and tested after the optimization study. The optimized harvester using three stacked opposing permanent magnets could achieve a normalized power density of 12655 $\mu Wcm^{-3}g^{-2}$ at 9.9 Hz frequency with 0.22g acceleration, which is significantly higher than other reported electromagnetic vibration energy harvesters.

Keywords Electromagnetic Vibration Energy harvester, Magnetic Spring, Finite Element Analysis, Analytical Modelling, Optimization

1. Introduction

There is rapidly growing interest in the field of autonomous sensor module networks in applications such as medical implants, portable electronics, machine monitoring, water/air quality monitoring, embedded sensors in buildings, and remote sensing, etc. Powering such wireless sensor networks is usually done through batteries because the mains power supply is inconvenient to access or unavailable [1]. Various types of energy harvesters have been proposed to power wireless sensor modules with an aim to eliminate batteries entirely or to extend the battery life. Energy can be scavenged from various ambient energy sources using different techniques. Ambient kinetic energy can be harvested using three main energy harvesting techniques, including electromagnetic (EM) [2-14], piezoelectric [15-18]and electrostatic [19-20]. Solar or light energy can be scavenged using solar cells [21-23] and ambient thermal energy can be scavenged using thermoelectric generators [24-25].

A significant amount of research has been carried out on different techniques of harvesting low frequency vibration energy over the last decade, for example, Saha et al. [4] demonstrated in their work that 300 μW - 2.5 mW of power could be generated by an AA battery size vibration energy harvester from human motion. The device developed by Manuel Gutierrez et al. could generate 101 μW when the load resistance was 1700 Ω with an acceleration of 0.1 g at 8.2 Hz. Halim et al. [9] designed an AAA battery size (3.9 cm^3) energy harvester, which could generate an average power of 203 μW, 32 μW and 78 μW from handshake, walking and jogging, respectively. Khan et al. [7] designed a cantilever structure to harvest bridge vibration energy. When the wing length was 86.8 mm, the vibration frequency was 7.6 Hz, and the acceleration was 0.6 g, the harvester could generate 2.214 mW power. The structure designed by Kurt et al. [10] could generate 14 mW with a load resistance of 35 Ω at a vibration frequency of 16 Hz.

In order to improve the energy conversion efficiency of the harvester, Wei Wang et al. [11] designed a tube shape

generator that can be extended at both ends to increase the range of motion of the moving mass. Song Hee Chae et al. [12] added ferrofluid to the generator to reduce friction, which was capable to generate 493 μW RMS power when the vibration frequency was 13 Hz, and the acceleration was 3 g . C. Drezet et al. [13] added a suspension system with the concept of high static and low dynamic stiffness to the generator. Adding a negative stiffness component in parallel with the positive stiffness of a linear oscillator could lower generator's resonant frequency while maintaining a small static displacement.

In order to collect kinetic energy from motions with a vibration frequency of less than 10 Hz, e.g. human movement such as jogging and walking, a magnetic spring was used instead of traditional mechanical springs [9, 26-27]. Kai Sun et al. [14] made a harvester based magnetic spring structure, which is suitable for human wrist vertical shaking. It could generate 50 mW RMS power, when the vibration frequency was 3.33 Hz, and the acceleration was 0.8 g. Compared with mechanical springs, the magnetic spring is not affected by material fatigue effect [3]. Additionally, the removal of mechanical spring can provide a low spring constant, leading to a low resonant frequency [28]. Hence, a magnetic spring was also applied in this work. Different from the prior arts, only a single magnet is fixed at the bottom of the harvester in this development in order to lower the resonant frequency. The moving mass used in this work consists of two or more adjacent magnets repelling each other in order to increase the density of the magnetic flux [4].

In the development of electromagnetic vibration energy harvesters, the main challenge is to achieve a high power density with certain constraints, such as the size of permanent magnet(s), the number of coil turns, the vibration frequencies, etc. Therefore, it is important to model and simulate the performance of the harvester. Berdy *et al.* [28] used mathematical equations to model and predict the optimal winding position. Its harvester could generate 304μW RMS power, when the vibration frequency was 6.7 Hz, and the acceleration was 0.075g. However, the number of suspension magnets is not optimized, and the mathematical modeling is too complex. It is evident from the literature that numerous research investigations have been undertaken on developing electromagnetic energy harvesters [2-5, 11, 26, 29-32], but there has been less attention paid on how to achieve high power density. Moreover, most of the models reported were frequency-domain models for standard sinusoidal vibration harvesters[33].

This work started with the development of an analytical model for an electromagnetic energy harvester which had a single magnetic spring and a pair of opposing permanent magnets. Unlike prior studies, the size of the generator in this study was limited to AA battery size to allow for direct battery replacement. A single magnetic spring was used to suit the low frequency application, and the opposing permanent magnets were used to give high flux gradient. In this development, in order to model the non-ideal sinusoidal vibration of the proposed harvester structure, we used Finite Element Analysis (FEA) and Simulink to develop a time-domain analytical model. The developed time-domain model is easier to implement than the numerical calculation method proposed in [28], leveraging the powerful built-in functionalities of Simulink. At the same time, the mechanical damping of the system was analyzed to improve the accuracy of the analytical model. The model was further applied to optimize the number of suspended magnets. The optimized harvester using three stacked opposing permanent magnets achieved the highest normalized power density among the reported electromagnetic vibration energy harvesters.

The paper is organized as follows: Section 2 presents the structure of the harvester. The Modelling theory and the FEA simulation of the proposed harvester structure are discussed in section 3. The fabrication of the energy harvester prototype, testing, results analysis, and model validation are detailed in section 4. The model application in the energy harvester optimization, the measurements of two optimized harvesters, and the results analysis are given in section 5. The normalized power density of the optimized harvester is also compared with the results reported in the literature. Finally, conclusions are given in Section 6.

2. Initial Generator Structure

In order the develop and verify the analytical model, an initial prototype was built and characterized.

Fig.1 shows the proposed structure of the vibration energy harvester operating at low frequency. It shows that the moving mass consists of two repelling permanent magnets and one soft ferromagnetic disc. A disc made of soft ferromagnetic material is inserted between the two repelling magnets. Two opposing magnets were directly attached to the soft ferromagnetic disc. Although the two magnets are repelling each other, the attracting force between one magnet and the disc is greater than the repelling force between the two opposing magnets. Hence，all magnets in the moving mass were securely adhered to the soft ferromagnetic disc. A tube made of Teflon is used as the casing. A coil is wrapped around the vertical sidewall of the tube casing. A small magnet is fixed at the bottom of the casing to repel the moving mass which forms a magnetic spring, as shown in Fig. 1[4]. The reason to use a single small magnet at the bottom instead of using one at each end of the casing as a magnetic spring is to increase the vibration displacement and to have a low resonant frequency. The moving mass is suspended in the tube under the gravity and repulsive force.

The center of coil is aligned to the center of the ferromagnetic disc.

When the tube vibrates in the Z-axis direction, the moving mass vibrates along the tube. It changes the magnetic flux in the coils. The voltage induced in the coil is defined by

$$U_{coil} = -N\frac{d\emptyset}{dt} = -N\left(\frac{d\emptyset}{dz}\right)\left(\frac{dz}{dt}\right) \quad (1)$$

Where N is the number of coil turns, $\frac{d\emptyset}{dt}$ is the magnetic flux gradient in the Z-axis direction (assuming the mass moves only in the Z-axis direction), $\frac{dz}{dt}$ is the relative velocity of the moving mass to the tube. The following section will present the initial prototype which has been fabricated and tested to verify the model.

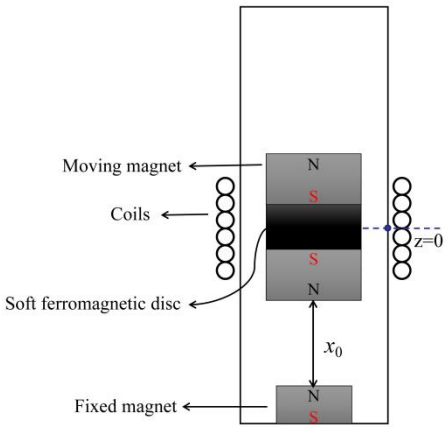

Fig. 1. The proposed structure of the energy harvester.

3. Modelling and Simulation

3.1 Harvester Dimensions

The height of the initial energy harvester in this development, Generator I, is chosen to be similar to an AA battery size and the overall generator dimension is D25.6mm×50mm. Each permanent magnet has a size of D19.05 mm × d6.35 mm × H6.35 mm separated by a D19.05 mm × d6.35 mm × H5 mm soft ferromagnetic disc, where D is the outer diameter, d is the inner diameter, and H is the height. FEA is used to simulate the average one turn magnetic flux along Z-axis. The parameters of Generator I are shown in Table 1.

Table 1. Generator I parameters

Parameters	Value
Moving mass (g)	33.60
Moving magnet size (mm)	D19.05 x d6.35 x H6.35
Fixed magnet size (mm)	D12.7 x d3.18 x H0.79
Tube (mm)	50
Coil outer diameter (mm)	12.8
Coil inner diameter (mm)	10.8
Coil Thickness (mm)	6
Coil diameter (mm)	0.09
Coil turns	1500
Coil resistance (Ohm)	300
Soft Ferromagnetic disc size (mm)	D19.05 x d6.35 x H5

3.2 Magnetic Flux Calculation

The magnetic flux distribution in Generator I has been extracted from FEA, which is shown in Fig. 2. In order to facilitate the development of analytical model for the energy harvester, the simulated magnetic flux distribution is further represented by an analytical equation, which is obtained by applying curve fitting techniques. The equation and all the coefficients obtained are given as followings:

$$\emptyset = \frac{a_0 + a_1\cos(\omega z) + b_1\sin(\omega z) + a_2\cos(2\omega z) + b_2\sin(2\omega z)}{1000} \quad (2)$$

Where, $a_0 = -0.003672$, $a_1 = 0.002152$, $b_1 = 0.06932$, $a_2 = -0.00176$, $b_2 = 0.02057$, $\omega = 0.182$.

As shown in Fig. 2, the curve fitting works well and can precisely represent the flux distribution.

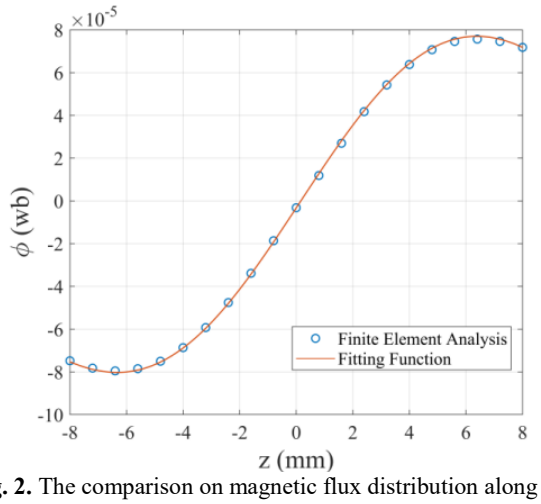

Fig. 2. The comparison on magnetic flux distribution along Z-axis between simulation and curve fitting.

3.3 The Force Analysis of Moving Mass

The harvester is excited by an external force, and it moves in sinusoidal motion. The external excitation frequency may change, pending on whether or not the external vibration source has a fixed frequency. The absolute motion of the tube can be expressed as

$$y(t) = A_m\sin(2\pi ft) \quad (3)$$

Where A_m is the external vibration amplitude, and f is the external vibration frequency.

In order to model the harvester, the force analysis of the moving mass is also required. Fig. 3 shows all the forces seen by the moving mass in the energy harvester. When the harvester is connected to a resistive load, R_{load}, the motion of the moving mass can be expressed as.

$$\ddot{z}(t) = \frac{F_{mag} - mg - C_e\dot{z} - F_f}{m} - \ddot{y}(t) \quad (4)$$

Where, F_{mag} is the repulsive force of magnet, F_f is the sliding friction, C_e is the electromagnetic damping coefficient, ~~A_m is the external vibration amplitude, f is the external vibration frequency,~~ m is the moving mass, z is the relative displacement between the moving mass and the tube.

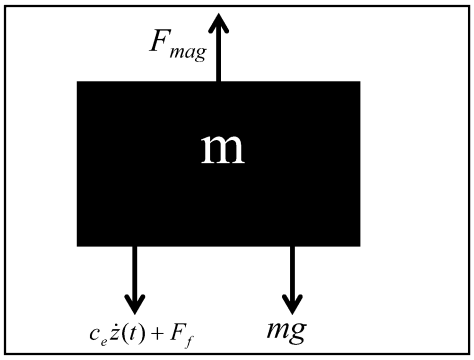

Fig. 3. Forces on the moving mass in a harvester.

3.4 Magnetic Force Calculation

The repulsive force caused by the bottom small magnet needs to be known in order to model the system motion as well as to calculate the induced voltage. FEA is used to simulate the relationship between the force F_{mag} and various displacement z. The equation based on Coulomb's theorem to fit the finite element simulation results is given as.

$$F_{mag} = \frac{\mu_0 m_1 m_2}{4\pi\left((z + x_0) \times 10^{-3}\right)^2 + s} \quad (5)$$

Where, z is the distance between the center of the tube and the center of the moving mass during vibration, x_0 is the distance between the lower magnet of the moving mass and the bottom magnet, as shown in Fig. 1, $(z + x_0)$ is the distance between the moving mass and the fixed magnet at the bottom, μ_0 is the vacuum permeability, m_1 and m_2 are the magnetization values at the magnet surface, and s is the offset used to match the simulation results. For a particular tube and moving mass, x_0 is a fixed value. In the case of Generator I, x_0 is 9.36 mm. From the curve fitting, following results can be obtained: m_1 = 28.07 A·m, m_2 = 23.2 A·m, s = 3.336×10^{-4}.

The curve of repulsive force versus displacement z from the FEA simulation along with the fitting curve are shown in Fig. 4. The fitting curve matches well with the FEA simulation results. To ensure the accuracy of the simulation, we measured the real repulsion force of the magnet in Generator I. The displacement and the corresponding force recorded in the experiment are also given in Fig. 4. It can be seen that the fitting curve matches well with the measured actual magnetic repulsive force and the simulated force from FEA. The curve in Fig. 4 indicates that the spring constant varies with displacement. A time-domain model is more suited to this structure than a conventional frequency-domain model.

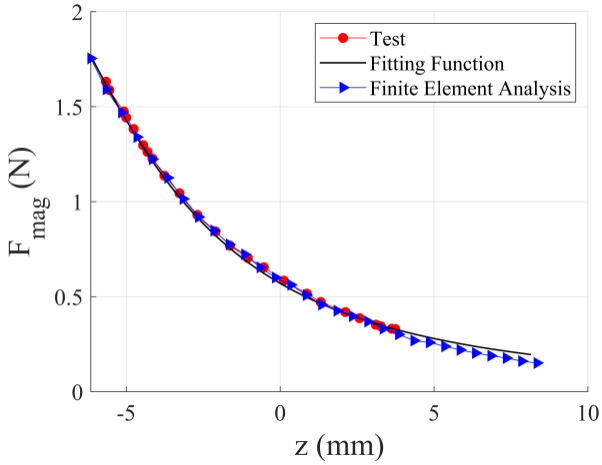

Fig. 4. The comparison on F_{mag} vs. displacement z.

3.5 Mechanical Damping Analysis

The mechanical damping in the generator includes the dry friction given by the inner wall of the pipe and the viscous friction caused by the air resistance. The dry friction is generally represented by Coulomb model [34], as shown below:

$$F_f = F_d \mathrm{sgn}\left(\dot{z}(t)\right) \quad (6)$$

Where F_d is a parameter to be identified, and sgn represents the signum function.

The sliding friction force is independent of the moving speed with the direction opposite to the moving direction. Therefore, the sliding friction can be expressed as.

$$F_f = \frac{\dot{z}(t)}{|\dot{z}(t)|} F_d \quad (7)$$

where, F_f is sliding friction, $\dot{z}(t)$ represents the relative velocity between the moving mass and the tube inner side wall.

The recorded decaying output voltage waveform of the generator after an impact shows linear attenuation rather than exponential decay. So, the main friction force of the system is the sliding friction of the inner wall of the tube and only

the dry friction is considered when modeling. The influence of air resistance is ignored.

F_d can be derived by analyzing the damping of the generator after an impact. According to the attenuation wave of voltage, the dry friction force can be solved by kinematic equation. Each peak of the voltage attenuation waveform is in the balance position, so the moving mass velocity corresponding to each peak can be calculated based on this. The acceleration caused by F_f, F_f/m, can be calculated using the two induced voltage peaks. The specific solution process is given by (8):

$$\frac{F_f}{m} = \frac{V_{pn} - V_{p0}}{nT} \tag{8}$$

Where V_{pn} is the velocity of the moving mass when the output voltage peaks after n^{th} cycle, and V_{p0} is the velocity of the moving mass at the first output voltage peak.

EQ(1) can be re-written as,

$$V_{pn} = \frac{U_{pn}}{N\frac{d\emptyset}{dz}}|z = z_0 \tag{9}$$

Hence, F_d can be obtained using:

$$F_d = |F_f| = m\frac{U_{pn} - U_{p0}}{N\frac{d\emptyset}{dz}\cdot nT}|z = z_0 \tag{10}$$

Where, z_0 is the coordinate of the balance position, ~~n~~ N is the number of turns of the coil, ~~V_{pn} is the velocity of moving mass when the output voltage of the n^{th} cycle is at the maximum value, and~~ U_{pn} is the maximum value of the output voltage ~~of the~~ after n^{th} cycle, and U_{p0} is the first peak value of the output voltage.

The comparison on the output voltage during the damping from both the model and the test is shown in Fig. 5 when calculated $|F_f|$ is used, i.e. 0.0028N. The oscillating frequency from the model is 5.5Hz, slightly lower than measured 6.3Hz, with approximate 12.7% discrepancy. A more sophisticated mechanical damping model is needed in the future for better accuracy.

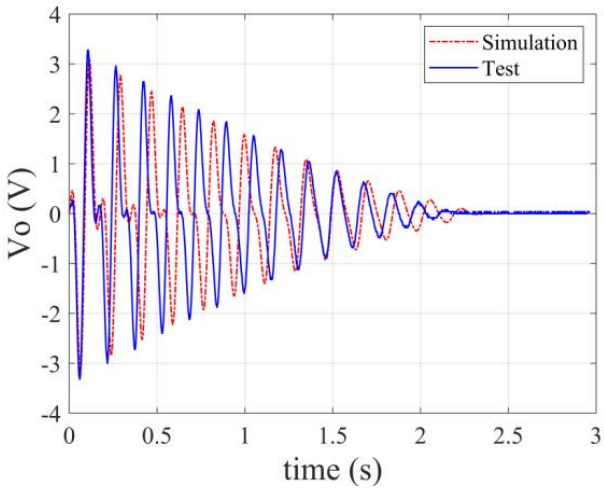

Fig. 5. Output voltage during the damping from model and test.

3.6 Electromagnetic Damping Calculation

The electromagnetic damping coefficient C_e is given as:

$$C_e = \frac{\left(N\frac{d\emptyset}{dz}\right)^2}{R} \tag{11}$$

The electromagnetic force, F_{em}, can be expressed as [5]:

$$F_{em} = C_e\dot{z}(t) = \frac{\left(N\frac{d\emptyset}{dz}\right)^2}{R}\frac{dz}{dt} \tag{12}$$

Where, N is the number of coil turns, R is the sum of coil resistance R_{coil} and load resistance R_{load}.

3.7 Model Implementation

Finally, all modules using corresponding equations and aforementioned parameters are put in place using ~~simulink~~ Simulink tool, MATLAB. All modules are integrated to form a complete energy harvester analytical model. The flow chart of the energy harvester model is shown in Fig. 6. The dimensions of all constructing objects and relevant parameters are listed in Table 1.

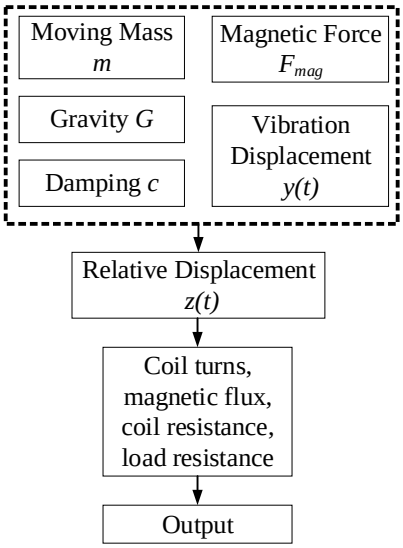

Fig. 6. The flow chart of the model.

4. Comparison of Test Results and Simulation

The energy harvester, Generator I, has been built using parameters given in Table 1. The fabricated Generator I prototype is shown in Fig. 7. In order to validate the analytical model, a series of experiments have been conducted. The test setup is shown in Fig. 8, including an accelerometer, a controllable shaker, a signal generator, a power amplifier and an oscilloscope. In the experiments, the harvester is fixed on the shaker, and the vibration acceleration is varied by adjusting the signal generator. The accelerometer is used to obtain the acceleration level, and the oscilloscope records the output voltage.

Firstly, the acceleration level is kept constant at 1 m/s^2 while only sweeping the vibration frequency of the shaker. Since the coil resistance of the generator is 300 Ohm, the maximum output power can be obtained when the load resistance is equivalent to the coil resistance. Among the resistors available commercially, the resistance value of 330 Ohm is the closest. Hence, the resistance of 330 Ohm is chosen as the load resistance R_{load} in the experiment. The effective value of output voltage of the harvester with 330 Ohm R_{load}, V_{rms}, is recorded at different frequencies. The measured and simulated values of V_{rms} at different frequencies are shown in Fig. 9. The purpose of this experiment is to find the resonant frequency of the generator. As can be seen in Fig. 9, the induced voltage reaches maximum at 6 Hz in the experiment. But in the simulation, the maximum occurs at 5.5 Hz. The discrepancy is similar to the phase difference found in Fig. 5.

Fig. 7. The fabricated harvester prototype.

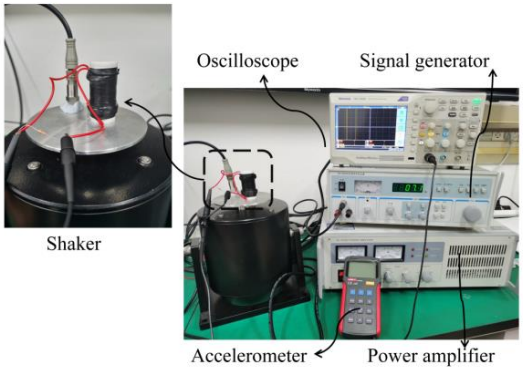

Fig. 8. Measurement set-up.

The harvester was further tested under two randomly selected conditions. Firstly. a peak vibration acceleration of 7.5 m/s^2 was applied at 10.6 Hz with R_{load} = 330 Ohm. Secondly, a peak vibration acceleration of 9.9 m/s^2 was applied at 12.4 Hz with R_{load} = 330 Ohm. The actual output waveform was recorded by oscilloscope, as shown in Fig. 10 and Fig. 11. The test and simulation output waveforms are given in Fig. 10 and Fig. 11. The comparison between the measured output voltage waveform and corresponding calculated output voltage waveform indicates that the analytical model can accurately predict the electrical performance of the energy harvester.

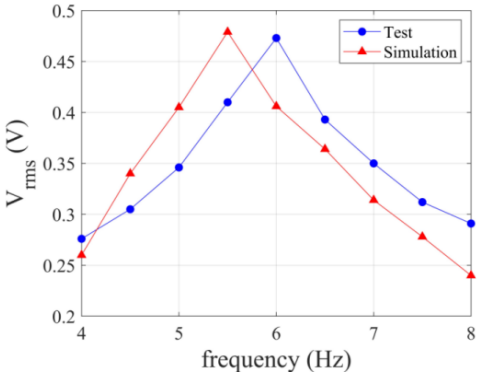

Fig. 9. Simulated and tested output voltage V_{rms} at various frequencies with 1 m/s^2 peak acceleration and 330 Ohm R_{load}.

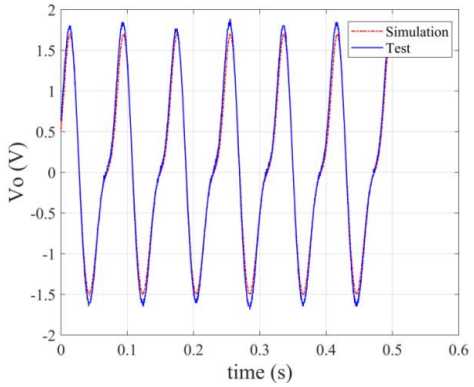

Fig. 10. Tested and simulated output voltage when 7.5 m/s^2 acceleration, 10.6 Hz vibration, 330 Ohm R_{load}.

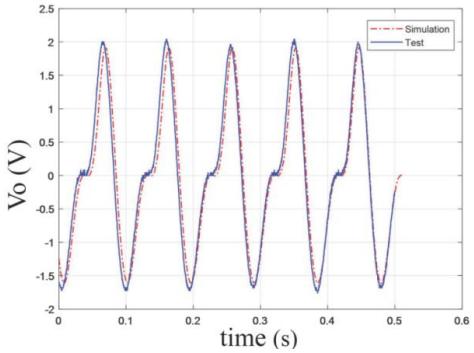

Fig. 11. Tested and simulated output voltage when 9.9 m/s^2 g, 12.4 Hz vibration, 330 Ohm Rload.

The test results obtained under load condition show that the model can accurately predict the actual output voltage of the generator. However, as shown in Fig. 9, the calculated resonance frequency of the harvester is slightly different from the measured resonant frequency. The reason for this phenomenon is that the mechanical damping is simplified in the analytical model. In the future, a more complex model for the mechanical damping is required to reduce this discrepancy. Fortunately, the electromagnetic damping is far greater than the mechanical damping under load condition, which makes the discrepancy negligible when predicting the output voltage. As shown in Fig. 10 and Fig. 11, the simulated output voltage waveform matches the actual output voltage waveform very well at any frequencies. Hence, we can use this validated modeling method to start the optimization work.

5. Optimization and Test

5.1 Optimization

The previous Sections have given the details of the model development and validation for Generator I. The validated model can be applied to optimize the harvester's structure and parameters, such as the number of magnets, the size of soft magnetic disc. The moving magnets of Generator I has a small thickness. There is plenty room for larger magnets for the same size of tube. Therefore, we increase the thickness of every moving magnet from 6.35 mm to 9.525 mm to construct Generator II, in which everything else is kept the same. The parameters of Generator II are shown in Table 2. On the basis of Generator II, the generator is further optimized by changing the thickness of magnets and ferromagnetic discs as well as the number of magnets and discs while keeping the total thickness of the moving mass constant. The number of the magnets in the moving mass is varied from 2 to 5 in the optimization study. The corresponding types of generator in the optimization study, from type II to type V, are shown in Fig. 12. A generator using a single magnet, i.e. type I as shown in Fig. 12, is also added for comparison purpose only.

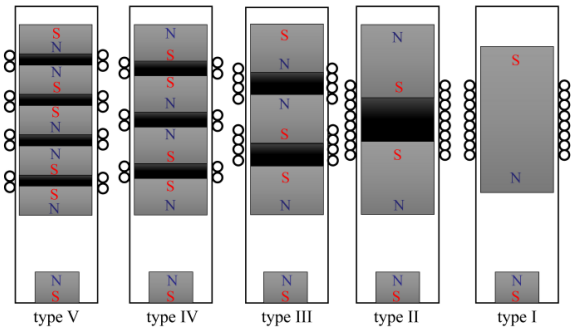

Fig. 12. Five types of harvester structures.

The relationship between magnet repulsion force and the displacement in z-direction for all five types of structures in Fig.12 is obtained by finite element simulation. The simulation results are shown in Fig. 13. The horizontal solid line represents the gravity of the suspended block in type II to type V, and the horizontal dotted line represents the gravity force of the suspended block in type I. The intersection of the horizontal line and the curve is the equilibrium point, and the z-axis coordinate of the equilibrium point is defined as Z_0. The equilibrium point Z_0 of all structure from type I to type V are 2.5mm, 2mm, 0.5mm, -1mm, -2mm.

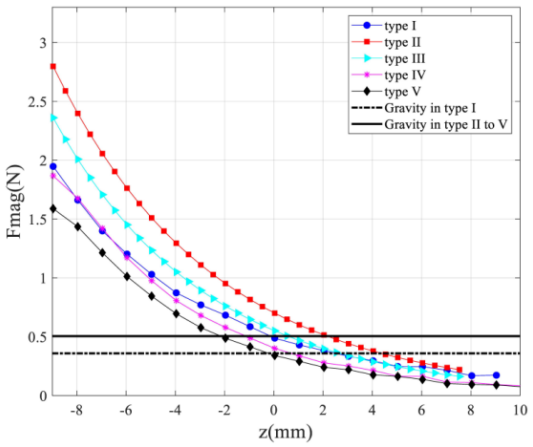

Fig. 13. The relationship between magnet repulsion force and the z-direction displacement under five structures.

The resonant frequency of a magnetic spring structure can be found by [28]:

$$f_{res} = \frac{1}{2\pi}\sqrt{\frac{k_{mag}(Z_0)}{m}} \quad (13)$$

Where, $k_{mag}(Z_0)$ is the spring constant at static equilibrium, also the derivative of magnetic force with respect to displacement at Z_0, m is the mass of the levitating magnet. It should be noted that this estimation is accurate only for small displacement. The resonant frequency may change at large displacements due to the nonlinear nature of the magnetic force.

The estimated resonant frequencies of structures from type I to type V are 4.89Hz, 6.49Hz, 6.36Hz, 6.6Hz and 6.63Hz respectively.

Fig.14 shows the change rate of magnetic flux in the coil with Z-direction displacement corresponding to the five structures obtained from finite element simulations. It can be seen from the figure that type V has the highest change rate of magnetic flux. In other words, if the suspension magnet passes through the coil plane at the same velocity, type V will produce the highest output voltage. At the same time, it can be seen from the FEA results that the maximum change rate of magnetic flux of each generator appears in the center of their respective coils.

Following the same modeling steps described above, five types of generators shown in Fig. 12 are modeled and compared. The predicted peak output voltage under load condition for all these five types of generator are shown in Fig. 15. In this comparison, an external vibration acceleration of 0.5m/s^2 and a 330 Ohm load resistance with the vibration frequency varying from 3.4 Hz to 9.9 Hz are used.

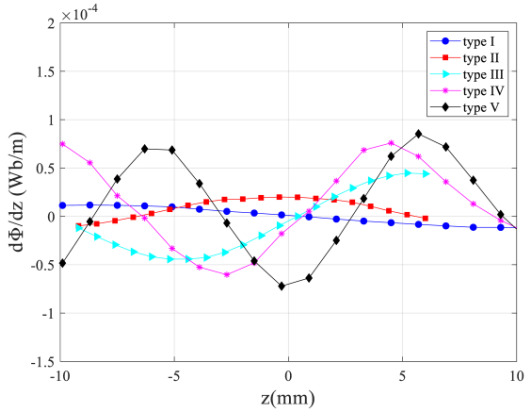

Fig. 14. The change rate of magnetic flux in the coil with Z-direction displacement for the five structures.

It can be seen from Fig. 15 that the resonant frequencies of generators from type II to type V are very similar because the moving mass of these types is kept the same in the study and the spring constant is similar. From type II to type IV, the output voltage of the harvester increases significantly with the increase of the number of magnets. The output voltage of type V is the highest at resonant frequency. This is consistent with the analysis in Fig. 13 and Fig. 14.

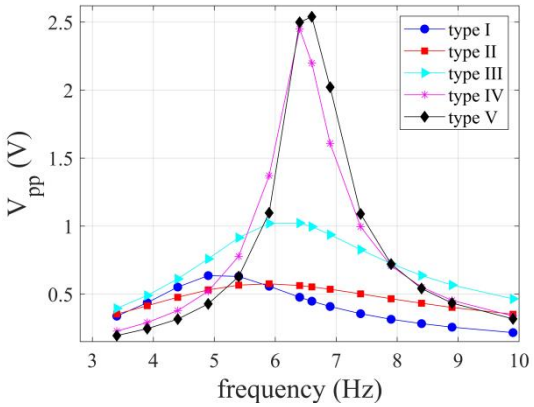

Fig. 15. Predicted peak output voltage for all five generators at various frequencies with 0.5m/s^2 g and 330 Ohm R_{load}.

For large displacement vibration, because the magnet moves away from the current coil center to another coil region, the output will be reversed, and then the effective output will be reduced. Based on the optimization study and the commercially available hard magnets and ferromagnetic discs, both type II and type III designs have been chosen for prototyping. The parameters of Generator II are based on type II design with all parameters already given in Table 2. Generator III is based on design type III, which has a double coil structure (each coil having 750 turns) with 4 mm thickness ferromagnetic disc. The parameters used for Generator III is also given in Table 2.

Table 2. Generator parameters

Parameters	Generator II	Generator III
Moving mass (g)	51.47	51.47
Moving magnet size (mm)	D19.05 x d6.35 x H9.525	D19.05 x d6.35 x H6.35
Fixed magnet size (mm)	D12.7 x d3.18 x H0.79	D12.7 x d3.18 x H0.79
Tube (mm)	50	50
Coil outer diameter (mm)	12.8	12.8
Coil inner diameter (mm)	10.8	10.8
Coil Thickness (mm)	6	3
Coil diameter (mm)	0.09	0.09
Coil turns	1500	750 x 2
Coil resistance (Ohm)	300	300
Ferromagnetic disc size (mm)	D19.05 x d6.35 x H8	D19.05 x d6.35 x H4

5.2 Comparison between Generator II and Generator III

The structure of Generator II and Generator III is shown in the Fig. 16. Both Generator II and Generator III have been tested on the shaker. Fig. 17 shows the measured open circuit voltage, V_{pp}, at different vibration frequencies with 0.5 m/s^2 acceleration. Fig. 18 shows the tested effective output voltage at different vibration frequencies with 0.5 m/s^2 acceleration and 330 Ohm R_{load}. As shown in Fig. 17, the V_{pp} of output voltage is 7.68 V and 7.93 V for Generator II and Generator III at their respective resonant frequencies. The tested resonant frequencies under open circuit condition are close to the model prediction. The output voltage of Generator III is higher than that of Generator II at most frequencies tested. And as shown in Fig. 18, the RMS value of output voltage is 0.309 V and 0.412 V for Generator II and Generator III at their respective resonant frequencies.

Compared with Generator II, the RMS output voltage of Generator III is increased by 33.3%. However, the tested resonant frequencies under load condition have been unexpectedly shifted to lower values, which needs to be investigated further in the future.

Fig. 19 shows the output voltage waveform from both the model and the measurement of Generator II with 2.2 m/s^2 acceleration, 9.9 Hz vibration frequency, and 330 Ohm R_{load}. Fig. 20 shows the output voltage waveform from both the model and the measurement of Generator III at the same condition. According to the test results shown in Fig. 19 and Fig. 20, the peak to peak output voltage, V_{pp}, of Generator II and Generator III are 1.78 V and 2.12 V, respectively. Generator III has better output characteristics than Generator II with the peak to peak output voltage value increased by 19.1%.

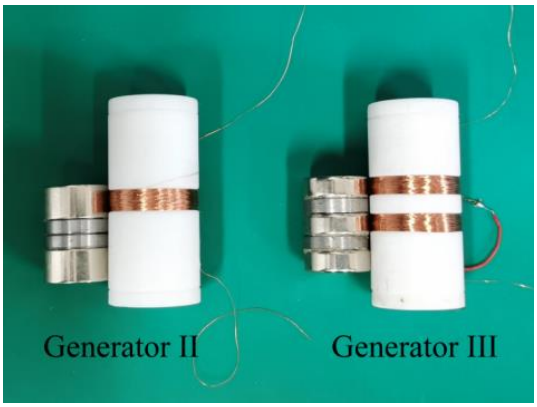

Fig. 16. The structure of Generator II and Generator III.

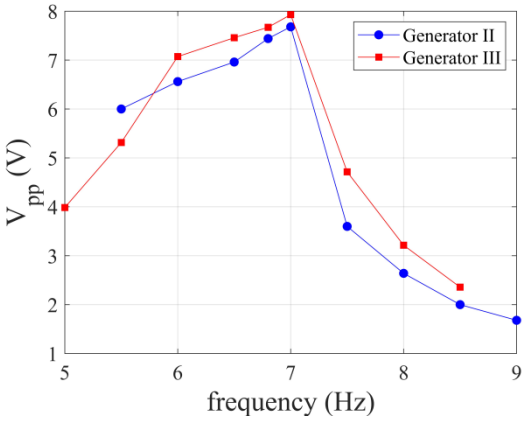

Fig. 17. Measured open circuit voltage, V_{pp}, at various vibration frequencies with 0.5 m/s^2 acceleration.

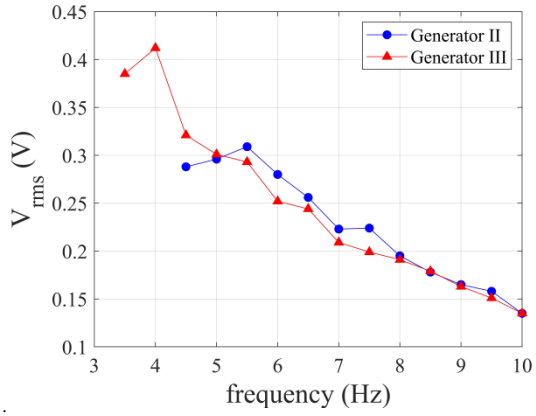

Fig. 18. Measured output voltage, V_{rms}, at different vibration frequencies with 0.5 m/s^2 acceleration and 330 Ohm R_{load}.

Comparing the results between model and test, the peak to peak output voltage of Generator II obtained from model is 1.63 V with a discrepancy of 8.4% to the measurement. The peak-to-peak output voltage of Generator III obtained from model is 2.128 V with a discrepancy of 0.38% to the measurement. The comparison again confirms that the analytical model developed can accurately predict the performance of the generators.

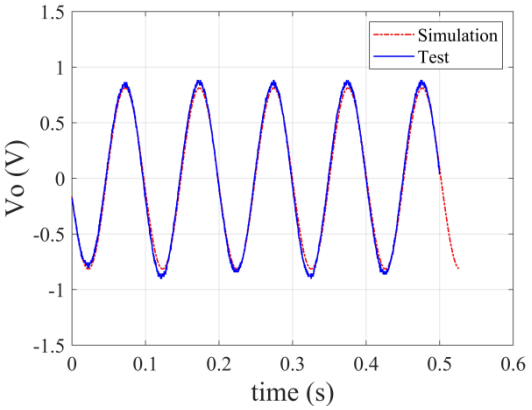

Fig. 19. Output voltage waveform obtained on Generator II from both model and measurement with g = 2.2 m/s^2, f = 9.9 Hz , R_{load} = 330 Ohm.

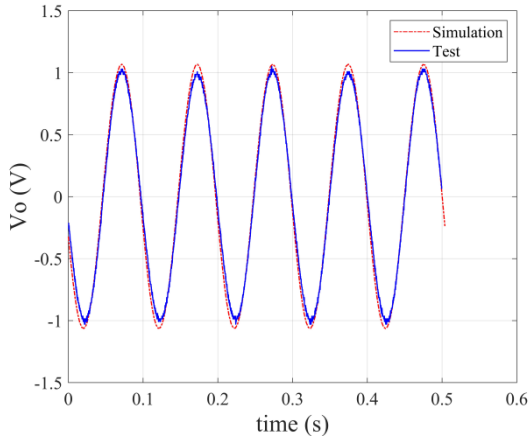

Fig. 20. Output voltage waveform obtained on Generator III from both model and measurement with g = 2.2 m/s^2, f = 9.9 Hz, R_{load} = 330 Ohm.

A comparison on the measurement results between the energy harvesters developed in this work and other electromagnetic energy harvesters reported in the literature is given in Table 3. For comparison purpose, a commercial electromagnetic vibration energy harvester from Ferro Solutions [35] typically operating in the frequency range of 20 -120 Hz is added in Table 3. The power density (PD) included in the comparison is one of the important parameters, which is defined as the measured power output divided by the volume of the device. The normalized power density (NPD) included in the table is also a key parameter, which is the power density divided by the acceleration level squared. Because power output is proportional to acceleration squared, the normalized power density gives a fairer comparison between devices than the power density[28]. Hence, the normalized power density is chosen as the Figure of the Merit (FOM) in this study.

In [12], the generator could generate 2.82 μWcm^{-3}g^{-2} NPD when the vibration frequency was 13 Hz, and the acceleration was 3g. In [14], the generator could generate 2500 μWcm^{-3}g^{-2} NPD when the vibration frequency was 3.33 Hz, and the acceleration was 0.8g. In [28], the generator could generate 7000 μWcm^{-3}g^{-2} NPD when the vibration frequency was 6.7 Hz, and the acceleration was 0.075g. In this work, the developed Generator III shows the highest reported NPD of 12665 μWcm^{-3}g^{-2} thanks to the optimization study and the special structure using stacked opposing magnets. The validated analytical model can be applied to further investigate the impact of the height of the coil and the thickness of the soft ferromagnetic disc on the output power. On the basis of Generator III, the height of the coil and the thickness of the soft ferromagnetic disc can be varied in the analytical model. The corresponding RMS output power is obtained under 0.5 m/s^2 acceleration at its resonant frequency with matched load resistance, as shown in Fig. 21.

The change of coil height will lead to the flux linkage change of the coil. When the coil height decreases from 5 mm to 2 mm, the magnetic flux linkage of the coil increases gradually. Similarly, the increase of the thickness of the ferromagnetic disc leads to the increase of the magnetic flux inside the coil, the repulsive force between the suspended magnet and the fixed magnet at the bottom, and the mass of the suspended object. According to equation (1) and equation (3), the change of the above parameters leads to the change of the RMS output power of the harvester, as shown in Fig. 21. The thickness of 4 mm used for the ferromagnetic discs in Generator III is the optimum value. If the height of the coil is reduced from 3 mm to 2 mm, the NPD of Generator III can potentially be further increased to 17194 μWcm^{-3}g^{-2} by 15.7%.

Table 3. Comparison of electromagnetic energy harvester measurement results from literature.

Accel. (g)	Freq. (Hz)	Vol. (cm3)	PD (μWcm-3)	NPD (μWcm^{-3}g^{-2})	RMS Power (μW)	Ref.
0.22	9.9	15.71	432.21	**8929.96**	6790	Gen. II
0.22	9.9	15.71	612.99	**12665.08**	9630	Gen. III
0.075	6.7	7.7	39.5	**7000**	304	[28]
0.1	6.7	7.7	53.2	**5300**	410	[28]
3	13	19.4	25.41	**2.82**	493	[12]
0.8	3.33	31.8	1572	**2500**	50000	[14]
0.1	60	170	30.59	**3059**	5200	[35]

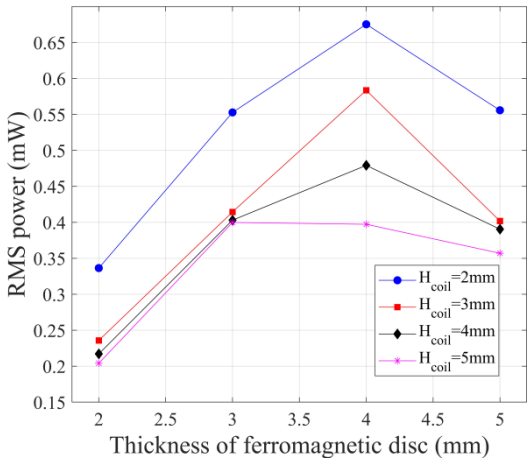

Fig. 21. The calculated RMS output power with different heights of coils and thickness of soft ferromagnetic discs.

6. Conclusion

This work introduces the development of a time-domain modelling method for a tube electromagnetic vibration energy harvester using stacked and magnetically levitated opposing permanent magnets. Finite element analysis (FEA) and Simulink simulation have been carried out to verify the theoretical model. An initial generator prototype with a pair of magnets repelling each other was built for model validation. The prototype was tested on a controllable shaker to obtain its output voltage and power level at different frequencies under a same acceleration. The measured results are critically analyzed and compared with the simulation results. The verified model was further applied in the harvester optimization by varying the thickness of magnets as well as the number of magnets stacked.

Two more generator prototypes were built and tested. Generator II is similar to Generator I, but with a pair of thicker magnets. Generator III has three magnets stacked with the same moving mass as that of Generator II. Both Generator II and Generator III were characterized. The output voltage V_{pp} of Generator II is 1.78 V with an acceleration of 2.2 m/s^2, R_{load} of 330 Ohm at 9.9 Hz. Compared with Generator II, the output voltage V_{pp} of Generator III is 2.12 V, increased by 19.1% at the same condition. The accuracy of the model is confirmed by the test results of the generators. The developed Generator III shows the highest NPD of 12665 $\mu Wcm^{-3}g^{-2}$ among the reported vibration energy harvesters using similar structures.

In the future, it is necessary to reduce friction as well as to improve magnetic flux linkage in order to further improve the performance of the generator. How to accurately measure and model the mechanical damping coefficient should also be considered in future modeling, so as to improve the accuracy of model for predicting harvester's open circuit characteristics.

References

[1] Y. Wang, Q. Zhang, L. Zhao and E.S. Kim, Non-resonant electromagnetic broad-band vibration-energy harvester based on self-assembled ferrofluid liquid bearing, J MEMS 4 (2017) 809-819.

[2] M. Gutierrez, et al, Design and characterization of a low frequency 2-dimensional magnetic levitation kinetic energy harvester, Sensors and Actuators A: Physical (2015) 1-10.

[3] D.F. Berdy, D.J. Valentino and D. Peroulis, Design and optimization of a magnetically sprung block magnet vibration energy harvester, Sensors and Actuators A: Physical (2014) 69-79.

[4] C.R. Saha, et al, Electromagnetic generator for harvesting energy from human motion, Sensors and Actuators A: Physical 1 (2008) 248-253.

[5] C.R. Saha, et al, Optimization of an electromagnetic energy harvesting device, IEEE Trans. Magn. 10 (2006) 3509-3511.

[6] M.A. Halim, D.H. Kim and J.Y. Park, Low frequency vibration energy harvester using stopper-engaged dynamic magnifier for increased power and wide bandwidth, Journal of Electrical Engineering and Technology 3 (2016) 707-714.

[7] F.U. Khan and M. Iqbal, Electromagnetic bridge energy harvester utilizing bridge's vibrations and ambient wind for wireless sensor node application, J. Sensors (2018) 1-18.

[8] F.U. Khan and I. Ahmad, Review of energy harvesters utilizing bridge vibrations, Shock Vib. (2016) 1-21.

[9] M.A. Halim, et al, A miniaturized electromagnetic vibration energy harvester using flux-guided magnet stacks for human-body-induced motion, Sensors and Actuators A: Physical (2016) 23-31.

[10] E. Kurt, M.M. Kale, S. Akbaba and N. Bizon, Analytical and experimental studies on a new linear energy harvester, CAN J PHYS 7SI (2018) 727-733.

[11] W. Wang, et al, Magnetic-spring based energy harvesting from human motions: Design, modeling and experiments, Energ. Convers. Manage (2017) 189-197.

[12] S.H. Chae, et al, Electromagnetic linear vibration energy harvester using sliding permanent magnet array and ferrofluid as a lubricant, Micromachines-Basel 10 (2017) 288.

[13] C. Drezet, N. Kacem and N. Bouhaddi, Design of a nonlinear energy harvester based on high static low dynamic stiffness for low frequency random vibrations, Sensors and Actuators A: Physical (2018) 54-64.

[14] K. Sun, G. Liu and X. Xu, in: Z. X. Hou (Ed.), Nonlinear

resonant generator for harvesting energy from human wrist vertical shaking, Applied Mechanics and Materials, vol. 128-129, 2012, pp. 923-927.
[15] M. Shirvanimoghaddam, et al, Towards a green and self-powered internet of things using piezoelectric energy harvesting, IEEE ACCESS (2019) 94533-94556.
[16] A. Khaligh, P. Zeng and C. Zheng, Kinetic energy harvesting using piezoelectric and electromagnetic technologies-state of the art, IEEE Trans. Ind. Electron. 3 (2010) 850-860.
[17] H. Xia, Y. Xia, Y. Ye, L. Qian, G. Shi and R. Chen, Analysis and simulation of synchronous electric charge partial extraction technique for efficient piezoelectric energy harvesting, IEEE Sens. J. 15 (2018) 6235-6244.
[18] S. Roundy and Y. Zhang, in: S. F. AlSarawi (Ed.), Toward self-tuning adaptive vibration based micro-generators, Proceedings of the Society of Photo-optical Instrumentation Engineers (SPIE), vol. 5649, 2005, pp. 373-384.
[19] Z. Wu, et al, Largely enhanced electrostatic generator based on a bipolar electret charged by patterned contact micro-discharge and optimized substrates, Nano Energy 104602 (2020).
[20] Y. Zhang, et al, Micro electrostatic energy harvester with both broad bandwidth and high normalized power density, App.l Energ. (2018) 362-371.
[21] S. Sadowski and P. Spachos, Solar-powered smart agricultural monitoring system using internet of things devices, 2018-01-01.
[22] S. Tang, et al, Smartmote: Energy and VoI aware solar-powered sensor network design for environment monitoring, 2012-01-01.
[23] C. Wang, et al, Combining solar energy harvesting with wireless charging for hybrid wireless sensor networks, IEEE T Mobile Comput. 3 (2018) 560-576.
[24] Y. Wang, et al, Flexible thermoelectric materials and generators: challenges and innovations, Adv. Mater. 180791629 (2019).
[25] X. Guo, et al, A new hybrid system composed of high-temperature proton exchange fuel cell and two-stage thermoelectric generator with Thomson effect: Energy and exergy analyses, Energy 117000 (2020).
[26] C.R. Saha, T. O Donnell, N. Wang and P. McCloskey, Electromagnetic generator for harvesting energy from human motion, Sensors and Actuators A: Physical 1 (2008) 248-253.
[27] S. Wu, et al, An electromagnetic wearable 3-DoF resonance human body motion energy harvester using ferrofluid as a lubricant, App.l Energ. (2017) 364-374.
[28] D.F. Berdy, D.J. Valentino and D. Peroulis, Design and optimization of a magnetically sprung block magnet vibration energy harvester, Sensors and Actuators A: Physical (2014) 69-79.
[29] Y. Pan, et al, Modeling and field-test of a compact electromagnetic energy harvester for railroad transportation, App.l Energ. (2019) 309-321.
[30] T. Lin, et al, Modeling and field testing of an electromagnetic energy harvester for rail tracks with anchorless mounting, Appl. Energ. (2018) 219-226.
[31] S. Wang, Y. Ke, P. Huang and P. Hsieh, Electromagnetic energy harvester interface design for wearable applications, IEEE T Circuits-II 5SI (2018) 667-671.
[32] C.R. Saha, et al, Optimization of an electromagnetic energy harvesting device, IEEE Trans. Magn. 10 (2006) 3509-3511.
[33] F.U. Khan and M. Iqbal, Electromagnetic bridge energy harvester utilizing bridge's vibrations and ambient wind for wireless sensor node application, J Sensors (2018) 1-18.
[34] P.L. Green, et al, On the identification and modelling of friction in a randomly excited energy harvester, J Sound Vib. 19 (2013) 4696-4708.
[35]http://www.industrycortex.com/datasheets/profile/1001410661 , VEH-460.